

Infrared detectors based on surface barrier structures with internal photoemission

A.V. Voitsekhovskii, A.P. Kokhanenko, and S.N. Nesmelov

Tomsk State University

V.D. Kuznetsov Siberian Physical-Technical Institute at the Tomsk State University

Received June 4, 2003

Infrared focal-plane arrays of semiconductor photodetectors are promising for remote sensing of the atmosphere and the Earth's surface. In this paper, threshold characteristics of new types of silicon detectors with internal photoemission are analyzed and methods for controlling the cutoff wavelength of such photodetectors are considered.

The use of array photodetectors in apparatus for remote sensing considerably extends their functional capabilities. Optical systems based on such photodetectors are capable to measure directly with high accuracy spatial distributions of emissive characteristics inside different atmospheric or surface regions. This allows determination of the time and coordinate dependences of such parameters as temperature and concentration of gaseous constituents that are needed in physical models of technogenic or natural atmospheric disturbances.

Because of technological problems arising when producing large-format arrays based on solid HgCdTe solution, about two decades ago an active search for alternative materials for focal plane arrays in up-to-date devices started.^{1,2} For radiation detection in the 3–5 and 8–12 μm atmospheric windows, it is promising to use silicon surface-barrier structures (Schottky barriers and heterotransitions) with internal photoemission. The application of the silicon technology permits creation of homogeneous monolithic large-format arrays of detectors of this type with highly stable characteristics and relatively low cost.

In this paper, we review briefly the state of the art in development of silicon IR photodetectors with internal photoemission, consider the methods for control of detector characteristics, and calculate the threshold characteristics for different-type detectors.

The first photoemission detectors were the silicide Schottky-barrier detectors. Figure 1 depicts the energy band diagram of the most widely used silicon detector with internal photoemission – *p*-type silicon – platinum silicide (PtSi/*p*-Si) Schottky-barrier detector operating in the spectral range of 3–5 μm . Detection with photoemissive detectors can be divided into the following stages: radiation absorption by free carriers (usually holes) in metal or in highly doped semiconductor (stage 1 in Fig. 1), transport of photoexcited holes in electrode (stage 2), and following internal emission (stage 3) through the potential barrier at the boundary.

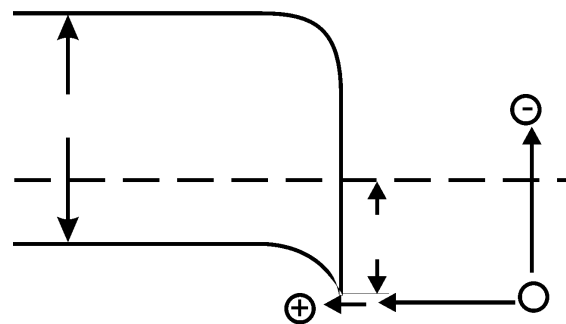


Fig. 1. Energy band diagram of PtSi/*p*-Si Schottky-barrier detector with internal photoemission.

The main characteristics of threshold properties of infrared detectors are the temperature of reaching the mode of background limitation (T_{bl}), at which the dark current is equal to the background photocurrent, the spectral detectability (D^*), and the noise equivalent temperature difference (NETD).^{1,3,4} The Table presents the boundary wavelengths (λ_c) and the background limitation temperatures for different silicide Schottky-barrier detectors. The value of T_{bl} was calculated at the entrance optics $F/2$, background temperature of 300 K, the effective Richardson constant $A^{**} = 4.4 \text{ \AA}/(\text{cm}^2 \cdot \text{K}^2)$, and the emission efficiency coefficient $C_1 = 0.2 \text{ eV}^{-1}$.

Parameters of Schottky-barrier detectors

Electrode	λ_c , μm	T_{bl} , K	Number of elements in array	Applications
Pd ₂ Si	3.5	133	5 · 2560, 4 · 5120 [Ref. 5]	Evaluation of Earth's resources from satellites
PtSi	5.5	101	1040 · 1040 [Ref. 6], 640 · 480 [Ref. 7]	Thermal imaging in the 3–5 μm spectral range
IrSi	8.5	76	128 · 128 [Ref. 8]	Thermal imaging in the 8–12 μm spectral range
CoSi ₂	2.8	149	–	Short-wavelength remote sensing
NiSi	3.1	142	–	

Nowadays several manufacturers in the U.S.A., Russia, and Japan produce monolithic PtSi arrays larger than 480×640 elements with NETD lower than 0.1 K (Refs. 6 and 7).

The lowest barrier height (0.152 eV) can be obtained in *p*-type silicon – iridium silicide (IrSi/*p*-Si) Schottky barriers.⁸ IrSi/*p*-Si detectors operating in the 8–12 μm range are not widely used because of the low quantum efficiency at the wavelengths longer than 8 μm, as well as because of some technological difficulties: poor reproducibility of the process of iridium silicide production, inhomogeneity in the properties of IrSi-detector arrays, problems in formation of a high-quality boundary interface.

The possibility of changing the potential barrier height at the electrode–silicon interface that determines λ_c of photoemissive detectors is important for optimization of detector characteristics as applied to particular conditions of radiation detection. For example, as the barrier height decreases, the characteristics of the detectors working in the evening and nighttime (at a lower background temperature) improve, but cooling the device to lower working temperatures is needed.

Initially, the height of the potential barrier (boundary wavelength) was changed through using as the electrode different silicides and silicide alloys or changing the technologies of silicide formation. For example, Ref. 11 reported production of a PtSi–IrSi detector with the 0.135 eV potential barrier. Later on it was shown that the effective height of the potential barrier can be changed through inhomogeneous doping of the near-surface silicon layer.^{12–17} The increase of the electric field near the barrier due to creation of a near-surface highly doped layer in a semiconductor also leads to reduction of the effective height of the potential barrier because of the Schottky effect.^{12,13} Formation of a highly doped near-surface layer allows λ_c of PtSi detectors to be increased up to 22 μm (Ref. 14), and that of IrSi detectors – up to 12 μm (Ref. 15).

The use of the molecular-beam epitaxy¹⁴ or low-energy ion implantation¹⁶ for creation of a highly doped near-surface layer is well known. Traditional boron implantation with the use of continuously working ion sources does not provide for the needed parameters of the highly doped zone because of defect formation at heating of the target surface by the ion beam and thermal-diffusion extension of the concentration profile.^{17,18}

We propose to use short-pulse boron implantation by the recoil nuclei method for creation of highly doped near-surface layers in silicon.¹⁷ The advantages of this method are simultaneous implantation and defect annealing in the surface silicon layer and wide capabilities of controlling the implantation conditions. To estimate the profiles of depth distributions of the doped boron at different implantation parameters, calculations with the direct analog model approximation were performed.¹⁸

Silicon plates of KDB-12 type coated by the cathode spreading method with a 10-nm boron layer

were irradiated by aluminum ions with the energy of 30–150 keV. The pulse number varied from 5 to 500 (ion flow of $2 \cdot 10^{12}$ ion/cm² per pulse). Irradiation was followed by etching of the boron film and annealing of samples in hydrogen vapor at the temperature of 500–800°C. The boron profiles were determined by the SIMS method. The electric parameters of the irradiated samples were studied by the contactless radiowave technique.¹⁸

As a result of experimental investigations, it was found that the short-pulse boron implantation by the recoil nuclei method followed by the annealing creates highly doped surface layers of 5–15 nm thickness with the admixture distribution of the exponential character and the surface concentration of 10^{18} – 10^{20} cm⁻³. In Ref. 19 the energy band diagrams of PtSi/Si Schottky barriers with a highly doped layer made by the recoil nuclei method were calculated and the dependence of λ_c on the layer parameters was determined. In Ref. 20 the spectral and threshold characteristics of detectors with the surface highly doped layers were calculated and it was shown that the boundary wavelengths of the PtSi/Si Schottky-barrier detectors can be increased up to 14 μm due to creation of the highly doped layer by the above method, and this provides for the increase of the quantum efficiency in the 3–5 μm spectral range.

New technological possibilities of controlling the boundary wavelength of photoemissive silicon detectors are presented by p^+ -Ge_xSi_{1-x}/*p*-Si heterotransitions, in which the height of the potential barrier at the heteroboundary depends on the germanium content and boron concentration in the germanium silicide film. Monolithic detectors with the boundary wavelength from 3 to 22 μm are now created based on GeSi/Si heterotransitions.^{9,10,21–23} Along with doping, in the process of epitaxial growth it is possible to employ the method of radiation doping by B the GeSi admixture for optimization of the detector spectral characteristic. The optimal thickness of the GeSi electrode is about 20 nm (the optimal thickness of the PtSi electrode is 2 nm (Ref. 1)), which is caused by the lower GeSi absorption coefficient. Single-layer GeSi-heterotransition internal photoemission photodetectors (HIP detectors) and Schottky-barrier detectors have the close values of A^{**} and C_1 .

An extra possibility to increase the internal quantum efficiency in HIP detectors is creation of structures with alternating layers of highly doped GeSi and lowly doped silicon. In many-layer HIP detectors, maximal values of C_1 achieved 1.4 eV^{-1} (Ref. 24). The promising direction of the up-to-date optoelectronics is the development of detectors with GeSi/Si quantum wells,^{25–28} as well as multispectral detectors based on PtSi/GeSi/Si and PtSi/Si/GeSi/Si structures,^{29,30} in which λ_c strongly depends on the bias voltage. In this connection, a large number of papers are devoted to the study of spectral properties of GeSi quantum well detectors and the technologies for formation of many-layer structures. The concept of application of GeSi/Si HIP detectors in the 3–5 μm range is now well developed.²⁵

Consider the threshold characteristics of silicon detectors with internal photoemission. For photoemissive detectors T_{bl} can be found from the equation³:

$$A^{**} T_{bl}^2 \exp\left(-\frac{1.24q}{\lambda_c k T_{bl}}\right) = C_3 C_1 \sin^2 \theta \int_0^{\lambda_c} \frac{t(\lambda) \left(\frac{1}{\lambda} - \frac{1}{\lambda_c}\right)^2}{\lambda^3 \left[\exp\left(\frac{C_2}{\lambda T_b}\right) - 1\right]} d\lambda,$$

where q is the electron charge; k is the Boltzmann constant; λ is the working wavelength; θ is the aperture half-angle; T_b is the background temperature; $C_2 = 1.43 \cdot 10^4 \mu\text{m}/\text{K}$, $C_3 = 37372 \text{ \AA}/(\mu\text{m}^4 \cdot \text{cm}^{-2} \cdot \text{eV})$; $A^{**} = 4.4 \text{ \AA}/(\text{cm}^2 \cdot \text{K}^2)$; $t(\lambda)$ is the atmospheric transmission coefficient.

The spectral detectability of photoemissive detectors is

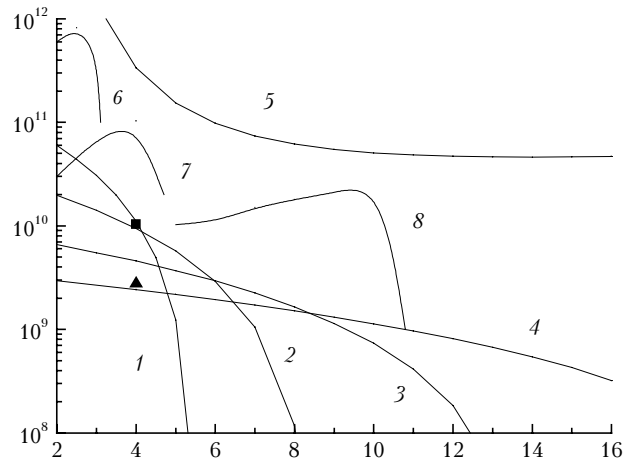


Fig. 2. Wavelength dependence of detectability for various-type photoemissive detectors.

$$D^*(\lambda) = \frac{C_1 t(\lambda) \lambda^2 \left(\frac{1}{\lambda} - \frac{1}{\lambda_c}\right)^2}{\sqrt{2q \left\{ A^{**} T^2 \exp\left(-\frac{1.24q}{\lambda_c k T}\right) + C_3 C_1 \sin^2 \theta \int_0^{\lambda_c} \frac{t(\lambda) \left(\frac{1}{\lambda} - \frac{1}{\lambda_c}\right)^2}{\lambda^3 \left[\exp\left(\frac{C_2}{\lambda T_b}\right) - 1\right]} d\lambda \right\}}},$$

where T is the detector temperature.

NETD of photoemissive detectors can be written as

$$\text{NETD} = \frac{(4F^2 + 1) \sqrt{\frac{2q}{S \tau_{ac}} \left\{ A^{**} T^2 \exp\left(-\frac{1.24q}{\lambda_c k T}\right) + C_3 C_1 \sin^2 \theta \int_0^{\lambda_c} \frac{t(\lambda) \left(\frac{1}{\lambda} - \frac{1}{\lambda_c}\right)^2}{\lambda^3 \left[\exp\left(\frac{C_2}{\lambda T_b}\right) - 1\right]} d\lambda \right\}}}{\int_0^{\lambda_c} \left[t(\lambda) C_1 C_2 C_3 \left(\frac{1}{\lambda} - \frac{1}{\lambda_c}\right)^2 \left\{ \lambda^4 T_b^2 \left[\exp\left(\frac{C_2}{\lambda T_b}\right) - 1 \right] \right\} \right] d\lambda}, \tag{3}$$

where $F = 1/2 \tan \theta$; τ_{ac} is the time of signal accumulation; S is the detector area.

The differences between various-type photoemissive silicon detectors will manifest themselves through the use of different λ_c , A^{**} , and C_1 in calculations.

Figure 2 depicts the wavelength dependence of D^* for photoemissive detectors: PtSi/ p -Si (curve 1), IrSi/ p -Si (curve 2), and PtSi/ p^+ -Si/ p -Si (curve 3) based on Schottky-barrier detectors, and many-layer p^+ -GeSi/ p -Si HIP detector (curve 4). For comparison, Fig. 2 also depicts the characteristics of an ideal photovoltaic detector (curve 5), InAs photoresistor (curve 6), and InSb (curve 7) and HgCdTe (curve 8) photodiodes.

The calculations were made for the following parameters: $\theta = 90^\circ$, $T = 80 \text{ K}$ (curves 1–3, 6–8) and 60 K (curve 4), $T_b = 300 \text{ K}$, $A^{**} = 4.4 \text{ \AA}/(\text{cm}^2 \cdot \text{K}^2)$,

$C_1 = 0.2 \text{ eV}^{-1}$ for curves 1–3 (Refs. 4, 8, 10, 14) and $C_1 = 1.4 \text{ eV}^{-1}$ for curve 4 (Ref. 24). In addition, Fig. 2 shows D^* at the wavelength of $4 \mu\text{m}$ for the multispectral PtSi/GeSi/Si detector at the bias voltage equal to zero (triangle) and 3 V (square) as calculated based on the data from Refs. 29 and 30.

It follows from Fig. 2 that the spectral detectability of photoemissive detectors is small as compared to the similar parameter for the detectors based on narrow band detectors (curves 6–8). This is explained by the low quantum efficiency of photoemissive detectors.

However, the accumulation mode of operation of the photoemissive detectors can provide for rather low values of NETD. Present-day technologies of the array photodetectors allow achieving the charge storage capacity in every element not exceeding $5 \cdot 10^7$

electrons. Maximal filling of the storage capacity at the high quantum efficiency typical of proper detectors is for the time much shorter than 1 ms. At a low quantum efficiency of the photoemissive detectors this time is much longer, which allows a considerable improvement of their threshold characteristics when operating with the frame frequency of 25–100 Hz.

Figure 3 depicts the NETD dependence on the boundary wavelength of photoemissive detectors. Three different cases were considered: $t(\lambda) = 1$ at any λ (curve 1); $t(\lambda) = 1$ in the 3–5 and 8–12 μm spectral ranges, and $t(\lambda) = 0$ at other λ (curve 2), $t(\lambda) = 1$ in the 8–12 μm spectral range, and $t(\lambda) = 0$ at other λ (curves 3–6). The calculations were carried out at the following parameters: $\theta = 90^\circ$, $T = 80$ K (curves 1 and 2) and 70 K (curves 3–5), $T_b = 300$ K, $A^{**} = 4.4 \text{ \AA}/(\text{cm}^2 \cdot \text{K}^2)$, $F = 2$, $C_1 = 0.2 \text{ eV}^{-1}$ for curves 1, 2, 4, 5 and $C_1 = 1.4 \text{ eV}^{-1}$ for curves 3 and 6, $S = 9 \cdot 10^{-6} \text{ cm}^2$. The accumulation time for curves 1–3, 5, 6 was equal to the time needed to fill the $5 \cdot 10^7$ electron well, if this time is shorter than 40 ms and 40 ms otherwise. For curve 4 $\tau_{\text{th}} = 10$ ms. Curve 6 is calculated neglecting dark currents.

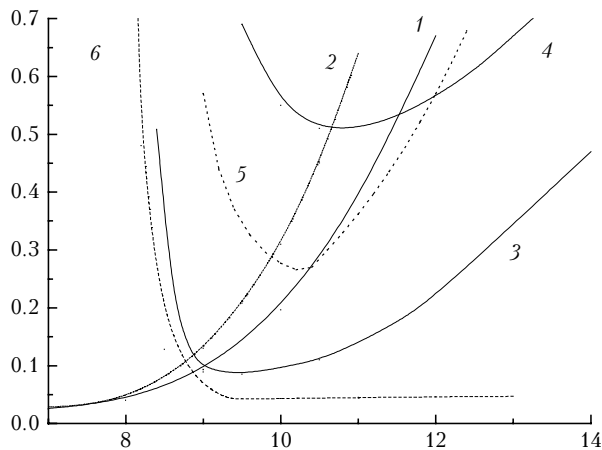


Fig. 3. Dependence of the noise equivalent temperature difference on λ_c for HIP detectors under different radiation recording conditions.

It follows from Fig. 3 that at the proper selection of the radiation recording conditions, photoemissive detectors provide for NETD values comparable with those of proper detectors based on narrow-band materials.¹ Worsening of NETD at large λ_c is associated with the increase of shot noise of the dark current at the decreasing height of the potential barrier and at small λ_c – with low values of the quantum efficiency near the long-wavelength boundary. The decrease of NETD can be obtained through decrease of the detector working temperature (curves 3 and 4). An important task is to select a technological cycle providing for the smallest A^{**} values and increase the emission efficiency coefficient C_1 through optimizing the design and parameters of detectors.

In the 8–12 μm spectral range, it is possible to use IrSi/Si Schottky-barrier detectors and GeSi/Si

HIP detectors. The best characteristics are provided by the HIP detectors because of the possibility of optimizing λ_c , well homogeneity and stability of properties. The NETD dependence on the boundary wavelength for photoemissive detectors in the 8–12 μm spectral range has a minimum, whose position depends on the temperature, detector parameters, and radiation recording conditions. Figure 4 depicts the dependence of optimal λ_c (curves 1, 2) and the corresponding NETD values (curves 3–7) for HIP detectors operating in the 8–12 μm spectral range. The calculations were made for the following parameters: $\theta = 90^\circ$, $T_b = 300$ K, $A^{**} = 4.4 \text{ \AA}/(\text{cm}^2 \cdot \text{K}^2)$, $S = 9 \cdot 10^{-6} \text{ cm}^2$, $F = 2$, $C_1 = 0.2 \text{ eV}^{-1}$ for curves 1, 3–5 and $C_1 = 1.4 \text{ eV}^{-1}$ for curves 2, 6, 7. Curves 5 and 7 are calculated neglecting the dark currents; for curve 4 $\tau_{\text{ac}} = 40$ ms, while for other curves it is 10 ms.

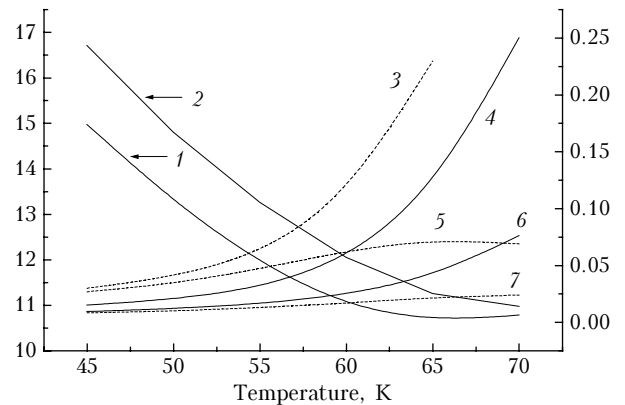


Fig. 4. Temperature dependence of optimal λ_c and minimal NETD for single-layer and many-layer HIP-detectors.

Thus, photoemissive silicon detectors yield in detectability to the detectors based on narrow-band ones and they require lower working temperatures. In spite of these disadvantages, photoemissive silicon detectors provide for rather small NETD values in the accumulation mode, possess high homogeneity and stability of properties, and give unique possibilities of using the well-developed silicon technology in production of array IR (1–23 μm) detectors integrated with the signal processing system in one crystal.

References

1. A. Rogalskii, *Infrared Detectors* (Gordon Press, London, 2001), 736 pp.
2. V.N. Sinita, ed., *Array Infrared Detectors* (Nauka, Novosibirsk, 2001), 376 pp.
3. A.V. Voitsekhovskii, A.P. Kokhanenko, S.N. Nesmelov, and V.N. Sokolov, *Izv. Vyssh. Uchebn. Zaved., Fiz.*, No. 5, 74–77 (2002).
4. M. Kimata and N. Tsubouchi, in: *Infrared Photon Detectors* (Optical Engineering Press, Bellingham, 1995), pp. 299–349.
5. J.R. Tower, A.D. Cope, L.E. Pellon, B.M. McCarthy, R.T. Strong, K.F. Kinnard, A.G. Moldovan, P.A. Levine, H. Elabd, D.M. Hoffman, W.M. Kramer, and R.W. Longsdorff, *RCA Review* **47**, 226–255 (1986).

6. N. Yutani, H. Yagi, M. Kimata, J. Nakanishi, S. Nagayoshi, and N. Tsubouchi, in: *IEDM Tech. Digest* (1991), pp. 175–178.
7. D.J. Sauer, F.V. Shallcross, F.L. Hsueh, G.M. Meray, P.A. Levine, H.R. Gilmartin, T.S. Villani, B.J. Esposito, and J.R. Tower, *Proc. SPIE* **1540**, 285–296 (1991).
8. B.-Y. Tsauro, M.J. McNutt, R.A. Bredthauer, and B.R. Mattson, *IEEE Electron Device Lett.* **10**, No. 7, 361–363 (1989).
9. H. Wada, M. Nagahima, and K. Hayashi, *Proc. SPIE* **3698**, No. 14, 584–595 (1999).
10. T.L. Lin and J. Maserjian, *Appl. Phys. Lett.* **57**, 1422–1424 (1990).
11. B.-Y. Tsauro, M.M. Weeks, and P.W. Pellegrini, *IEEE Electron Device Lett.* **9**, No. 2, 100–102 (1988).
12. J.M. Shannon, *Appl. Phys. Lett.* **24**, No. 8, 369–371 (1974).
13. H. Kanaya, F. Hasegawa, Yamaka, T. Moriyama, and M. Nakajima, *Jap. J. Appl. Phys., Pt. 1.* **28**, No. 4, 544–546 (1989).
14. T.L. Lin, J.S. Park, T. George, E.W. Jones, R.W. Fathauer and J. Maserjian, *Appl. Phys. Lett.* **62**, No. 25, 3318–3320 (1993).
15. B.-Y. Tsauro, C.K. Chen, and B.A. Nechay, *IEEE Electron Device Lett.* **11**, No. 9, 415–417 (1990).
16. C.-Y. Wei, W. Tantraporn, W. Katz, and G. Smith, *Thin Solid Films* **93**, 407–412 (1982).
17. A.V. Voitsekhovskii, A.P. Kokhanenko, A.G. Korotaev, and S.N. Nesmelov, in: *Proc. of the First International Congress on Radiation Physics, High Electronics, and Modification of Materials* (Tomsk, 2000), Vol. 3, pp. 362–364.
18. A.V. Voitsekhovskii, A.P. Kokhanenko, S.N. Nesmelov, S.I. Lyapunov, and N.V. Komarov, *Izv. Vyssh. Uchebn. Zaved., Fiz.*, No. 8, 11–20 (2001).
19. S.N. Nesmelov, A.V. Voitsekhovskii, A.G. Korotaev, and A.P. Kokhanenko, *Proc. SPIE* **4654**, 164–173 (2002).
20. A.V. Voitsekhovskii, A.P. Kokhanenko, S.N. Nesmelov, S.I. Lyapunov, and N.V. Komarov, *Izv. Vyssh. Uchebn. Zaved., Fiz.*, No. 11, 8–18 (2001).
21. V.I. Mashanov, I.B. Chistokhin, B.A. Zaitsev, O.P. Pchelyakov, L.V. Sokolov, E.G. Tishkovskii, B.I. Fomin, and E.I. Cherepov, *Mikroelektronika* **27**, No. 6, 412–418 (1998).
22. B.-Y. Tsauro, C.K. Chen, and S.A. Marino, *Opt. Eng.* **33**, No. 1, 72–78 (1994).
23. R. Strong, D.W. Greve, R. Misra, M. Weeks, and P. Pellegrini, *Thin Solid Films* **294**, 343–346 (1997).
24. J.S. Park, T.L. Lin, E.W. Jones, H.M. Del Castillo, T. George, and S.D. Gunapala, *Proc. SPIE* **2020**, 12–21 (1993).
25. H. Presting, *Thin Solid Films* **321**, 186–195 (1998).
26. R. People, J.C. Bean, C.G. Bethea, S.K. Sputz, and L.J. Peticolas, *Appl. Phys. Lett.* **61**, No. 9, 1122–1124 (1992).
27. D. Krapf, B. Adoram, J. Shappir, and A. Sa'ar, *Appl. Phys. Lett.* **78**, No. 4, 495–497 (2001).
28. J.S. Park, R.P.G. Karunasiri, and K.L. Wang, *Appl. Phys. Lett.* **60**, No. 1, 103–105 (1992).
29. J.R. Jimenez, *Proc. SPIE* **2225**, 393–403 (1994).
30. X. Xiao, J.S. Sturm, S.R. Parihar, S.A. Lyon, D. Meyerhofer, S. Paifrey, and F.V. Shallcross, *IEEE Electron Device Lett.* **14**, No. 4, 199–201 (1993).